

Global Ridge Orientation Modeling for Partial Fingerprint Identification

Yi Wang, *Member, IEEE*, and Jiankun Hu, *Member, IEEE*

Abstract—Identifying incomplete or partial fingerprints from a large fingerprint database remains a difficult challenge today. Existing studies on partial fingerprints focus on one-to-one matching using local ridge details. In this paper, we investigate the problem of retrieving candidate lists for matching partial fingerprints by exploiting global topological features. Specifically, we propose an analytical approach for reconstructing the global topology representation from a partial fingerprint. Firstly, we present an inverse orientation model for describing the reconstruction problem. Then, we provide a general expression for all valid solutions to the inverse model. This allows us to preserve data fidelity in the existing segments while exploring missing structures in the unknown parts. We have further developed algorithms for estimating the missing orientation structures based on some a priori knowledge of ridge topology features. Our statistical experiments show that our proposed model-based approach can effectively reduce the number of candidates for pair-wised fingerprint matching, and thus significantly improve the system retrieval performance for partial fingerprint identification.

Index Terms—Partial fingerprint identification, global ridge orientation estimation, model-based approach.

1 INTRODUCTION

Despite tremendous progress made in automatic fingerprint identification systems, matching incomplete or partial fingerprints such as latent prints remains a critical challenge today. Existing partial fingerprint algorithms concentrate on improving the accuracy of one-to-one matching based on local ridge details, i.e. Level 2 and Level 3 features. Jea and Govindaraju [1] addresses the problem by using localized secondary features derived from the relative information of minutiae points. Fang *et al.* [2] exploits representative points along ridge lines in addition to minutiae points and reports improved matching performance. Chen and Jain [3] investigates the extended Level 3 features of dots and incipient points to provide more information for partial fingerprint matching. However, the performance of their method depends on image quality as well as the number of high level features detectable in the partial fingerprint segments.

These ad hoc algorithms are designed on the basis of more delicate one-to-one comparisons. When used in one-to-many applications, they generally assume sequential matching or that the candidate list for such matching has already been established. However, sequential matching is not efficient for large-scale identification which can involve thousands or millions of records in the target database and retrieving a short and reliable list of candidates for matching is difficult in practice. As suggested by the NIST report *Concept of*

Operations (CONOPS) for Evaluation of Latent Fingerprint Technologies (ELFT) [4] published in 2007, automated search capabilities will assist latent experts by reducing the size of candidate lists they need to examine through elimination of the more obvious “nuisance” non-matches.

Recently, Feng and Jain [5] proposes a multi-staged filtering scheme to scan the database in search of the potential candidates for large-scale latent matching. However, the filtering algorithms rely on finding singular points in a partial fingerprint segment. When such critical information is not available, the scheme reduces to sequential screening.

In this paper, we propose to address the problem via a different approach by “supplementing” the partial fingerprint query first. In our previous work [9], we have developed a ridge orientation model that can comprehensively describe ridge orientation pattern inside a fingerprint image foreground. The orientation model clearly indicates that fingerprint global features are analytically describable. This means that, unlike the local features (e.g. minutiae points) whose distribution is regarded highly random, it is possible to predict the global topology pattern from incomplete information. Although we understand that fine ridge details cannot be recovered precisely in the missing parts, it is possible to reconstruct *topologically* the same pattern as of the original full print for conducting similarity searches in the database. The search outcome will yield a (preferably short) list of the most likely candidates for higher level matches. We call such a process as *candidate list retrieval*.

In this paper, we formulate the estimation of global ridge topology pattern as solving an inverse problem given incomplete orientation samples available in the partial fingerprint segments. We provide the general solution space for such an inverse model so that data

- Y. Wang is with the School of Mathematics and Statistics, The University of New South Wales, Sydney, Australia 2032.
E-mail: yi.wang@unsw.edu.au
- J. Hu is with the School of Computer Science and Information Technology, RMIT University, Melbourne, Australia 3001.



Fig. 1. Partial fingerprint examples: (a) a latent fingerprint [6], (b) a dabbed impression from sensor device [7] and (c) a contaminated image with unrecognizable parts [8].

fidelity can be preserved in a least square sense in the existing segments while reconstructing global topology representations. To estimate orientations in the unknown parts, we develop two ad hoc algorithms based on some *a priori* knowledge of fingerprint ridge topologies.

For performance evaluation, we conduct statistical experiments on partial fingerprint requests. In particular, we are interested in investigating how “small” a partial fingerprint could be for it to be inherently identifiable using our topology reconstruction method to conduct a successful candidate list retrieval. We call this the *lower bound* of the partial fingerprint image quality. We will evaluate the retrieval performance through fingerprint indexing [7], [10]. The indexing technique is useful for improving retrieval efficiency of fingerprint identification under normal circumstances [9], [11], [12]. To the best of our knowledge, it has not been investigated for partial fingerprint identification.

The problem with partial fingerprint queries in an indexing scheme is due to the fact that the indexing vector generated from the partial information can fall outside of the right candidate cluster in the search space. If we can correct the indexing vector of a partial fingerprint request after ridge topology reconstruction, we are able to improve the accuracy and efficiency of candidate list retrieval by minimizing the number of candidates that need to be examined in the database.

The rest of the paper is organized as follows. Section 2 introduces partial fingerprint scenarios and some general observations on global ridge topologies that can be utilized as a priori knowledge of fingerprints. Section 3 presents our inverse orientation model and provides a formula that governs the general solution space. Section 4 proposes two ad hoc algorithms based on the a priori knowledge of fingerprints. In particular, we investigate two mathematical models, namely the conditional cosine model and the fluid dynamic model, for estimating the missing peripheral structures in a fingerprint image. Section 5 reports our statistical experiments for performance evaluation, and finally we conclude our study in Section 6.

2 OBSERVATIONS OF FINGERPRINTS

Partial fingerprints can emerge from a number of scenarios. The most common case is in crime scene where latent prints are unwittingly left by friction ridge skin on a surface. Latent prints are often obscure and partial, which makes them difficult for identification especially against large-scale fingerprint databases.

Partial fingerprints are not restricted to latents. The problem also exists in small capturing devices. Although a compact 2D sensor is handy and cost-effective, it can only capture certain part of finger tip instead of full image from nail to nail. Therefore, one must take extra care for those acquired from such devices when matching them to full prints in an existing gallery database. In other scenarios, a fingerprint image may be damaged so much that it is inherently not recognizable in some areas. In such cases, it is better to disregard noisy regions and use only the recognizable parts for fingerprint identification. This process also generates partial fingerprints. Figure 1 illustrates partial fingerprint examples for these scenarios.

In many cases, the available partial segments may not accommodate sufficient ridge details for undertaking a normal matching process. In fact, matching error usually increases as the number of detected local features decreases [2], [3]. This is because verification must rely on precisely what *exists* in the partial fingerprint segments.

In the context of candidate list retrieval, however, the purpose is to narrow down search range in the database. This allows us to relax the accuracy requirements and estimate “what ought to be” in addition to what is available for retrieving a group of likely candidates for matching.

We notice that certain common features can be observed for the general ridge topology patterns of fingerprints. Fingerprints are often viewed as flow-like patterns. At the global level, ridge flows are generally smooth and continuous except near a few controlling points so called *singular points*. Therefore, it is not an unrealistic assumption that ridge flows are expandable to some extent at least in the “smooth” regions.

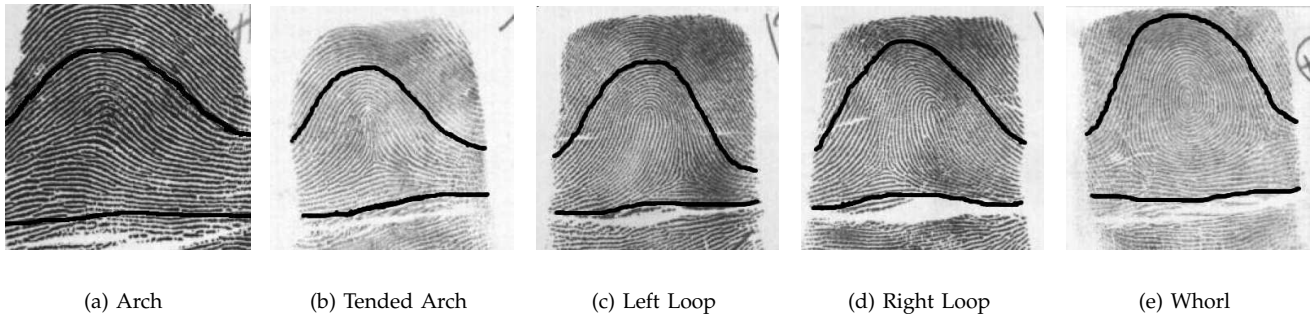


Fig. 2. Examples of peripheral arches in fingerprint topology patterns.

It can also be observed that ridge flows in the outer fingerprint regions generally exhibit some arch forms, even though the internal patterns can vary quite significantly from one to another. Figure 2 displays examples from five usual fingerprint categories, namely arch, tended arch, left loop, right loop and whorl. The peripheral arch trends are outlined in the fingerprint images.

We consider that the internal variation of ridge patterns is due to the presence of singular points, while the outer peripheral arch forms are caused by physical restrictions. Fingerprint is usually taken from above the first joint of a finger. As flexure creases appear at knuckles, the epidermal ridge lines also tend to be flat as they approach the knuckle furrows in the lower part of a fingerprint. Epidermal ridges on a finger tip, however, often exhibit curves flowing from one side of a finger to the other resulting in some arch forms surrounding the finger pad. Therefore, if a fingerprint is completely captured from tip to the knuckle furrow and rolled from nail to nail, it is reasonable to expect some general arch flows encompassing different singularity patterns in the fingerprint images.

Li and Yao [13] proposed a piece-wise linear model for predicting orientations in the outer regions of a fingerprint. This approach is not suitable to generate peripheral arches. First, the piece-wise linear model cannot guarantee the arch forms. Second, the approach needs exact information of singular points to partition a fingerprint image into multiple sectors and then apply a linear model to each of the sectors. However, partial fingerprints can have one or more singular points missing. Therefore, we must explore more suitable ways for describing the peripheral arch trends.

In the following, we shall first formulate an inverse orientation model for reconstructing global topology representations from partial fingerprints. Then, we will incorporate the a priori knowledge of ridge smoothness and peripheral arches into the modeling process.

3 INVERSE ORIENTATION MODEL

Ridge topology patterns are conventionally described by *ridge orientation field* - a 2D real-value matrix representation that accommodates the dominant ridge orientations

sampled at discrete positions in a fingerprint image. A number of mathematical models have been proposed in the literature for estimation of ridge orientations [14]–[17]. They generally materialize perceptions of ridge topology patterns from different perspectives.

In our previous work [9], we interpret the transformed orientation field as the phase portrait of a nonlinear dynamical system. The application of phase portrait models to flow-like textures was first introduced by Rao and Jain [18] in which a linear system was proposed to describe *local* orientations in a small neighborhood of oriented texture fields. Such a linear system can only describe a phase portrait with at most one critical point. Thus, it is not suitable for describing the global ridge orientation field of a fingerprint which often contains more than one singular points. There are some nonlinear dynamical systems proposed for texture analysis in the literature [19], [20]. However, they generally require prior knowledge of singular points whereas the singular point detection of fingerprints relies on an accurate orientation estimation in the first place. Moreover, solving these nonlinear systems can be difficult. For instance, simulated annealing is employed to optimize the model coefficient values in [19].

In [9], we proposed to approximate the global nonlinear dynamical system by Fourier series expansions, namely the FOMFE. Unlike other models, the FOMFE does not require any prior knowledge of the critical singular points for the entire modeling process. In fact, it is able to describe the overall ridge topology pattern seamlessly including all singularity regions. In our previous work [9], we have exploited the model coefficients to represent ridge orientation features and demonstrated a successful application in fingerprint indexing. In this paper, we propose to extend the modeling methodology by exploiting the predictive capability of mathematical modelling for partial fingerprint analysis.

Before we continue, it is necessary to provide a brief review of our approach and introduce some general terms. By doubling orientation angles, a fingerprint orientation field is transformed into a vector field which can be conveniently described by a system of partial differential equations $\dot{\mathbf{x}} = \mathbf{f}(\mathbf{x})$ with $\mathbf{x} = (x, y)^T$ being the

cartesian coordinates. In the FOMFE, we approximate the phase functions $\mathbf{f} = (f_c, f_s)^T$ using two bivariate trigonometric polynomials, respectively. For instance, in a defined and restricted two dimensional site, denoted $S : (-l \leq x \leq l, -h \leq y \leq h)$, we represent each phase function as

$$\begin{aligned} f(x, y) &= c_{00}\psi_{00}(x, y) + c_{01}\psi_{01}(x, y) + \dots \\ &\quad + c_{10}\psi_{10}(x, y) + \dots + \varepsilon(x, y) \\ &= \sum_{i=0}^{2k} \sum_{j=0}^{2k} c_{ij}\psi_{ij}(x, y) + \varepsilon(x, y), \end{aligned} \quad (1)$$

where $i, j, k < +\infty \in \mathbb{N}$ are polynomial orders, c_{ij} are real-valued model coefficients, and $\psi_{ij}(x, y)$ are expansion functions [9].

When input data is (evenly) sampled across the image site S , there is a unique best-fit solution to all data points in the sense of least-square error minimization. Therefore, (1) is indeed a truncated 2D Fourier expansion, and every estimated phase output is in the closed span \mathcal{V} of the expansion set $\Psi = \{\psi_{ij}(x, y)\}$ defined in S . In such a case, expansion coefficients $\{c_{ij}\}$ can be computed uniquely from *dual* functions of Ψ , denoted $\tilde{\Psi} = \{\tilde{\psi}_{ij}(x, y)\}$, for any $f(x, y) \in \mathcal{V}$ [21]. Since ψ_{ij} are orthogonal to each other, the dual functions can be evaluated by [21]

$$\langle \psi_{ij}(x, y), \tilde{\psi}_{kl}(x, y) \rangle = \delta = \begin{cases} 0 & (i \neq k, \quad j \neq l) \\ 1 & (i = k, \quad j = l) \end{cases}, \quad (2)$$

where $\langle \cdot \rangle$ is the integral inner product taken over the entire site S . Thus, according to [21],

$$c_{ij} = \langle \tilde{\psi}_{ij}(x, y), f(x, y) \rangle = \int_S \tilde{\psi}_{ij}^*(x, y) f(x, y), \quad (3)$$

where $(\cdot)^*$ denotes the complex conjugate operation. Since both ψ_{ij} and its dual $\tilde{\psi}_{ij}$ are real, the complex conjugate operation can be exempted. In practice, value of the modeling function $f(x, y)$ in (3) is replaced by the input phase data $d(x, y)$ sampled at that point.

3.1 Problem Formulation

If the phase samples are in a subset of the image site, i.e. $d(x, y) \in \Omega$ and $\Omega \subset S$, (3) becomes partial integral and the coefficient estimate c_{ij} is deviated from expectation. This situation typically happens for modeling partial fingerprints in which the partial segments are regarded as Ω . Let the remaining unknown region be defined as $\chi = \bar{\Omega}$ such that $\chi \cup \Omega = S$. Then, (3) is partitioned as

$$\begin{aligned} c_{ij} &= \sum_S \tilde{\psi}_{ij}(x, y) d(x, y) \\ &= \sum_{\Omega} \tilde{\psi}_{ij}(x, y) d(x, y) + \sum_{\chi} \tilde{\psi}_{ij}(x, y) d(x, y). \end{aligned} \quad (4)$$

Define $\beta_S = \{c_{ij} | S\}$ as the model coefficient set for the global phase portrait to be reconstructed, $\beta_{\Omega} = \{c_{ij} | \Omega\}$ as that evaluated from observation data in the partial

segment Ω , and $\beta_{\chi} = \{c_{ij} | \chi\}$ as that estimated for the unknown region χ . Then, (4) can be rewritten as

$$\beta_S = \beta_{\Omega} + \beta_{\chi}. \quad (5)$$

We interpret the problem of partial fingerprint reconstruction as how to reconstruct the global representation β_S from the partial evaluation β_{Ω} subject to all possible constraints imposed on β_{χ} . We name this formulation as the *inverse orientation model*.

The above formulation indicates that the solutions to (5) cannot be unique by fitting data in the existing subset Ω alone. This is because β_S is also affected by the uncertainty introduced by β_{χ} . In practice, however, if Ω dominates the site S , the partial representation β_{Ω} can serve as a good approximation to the global representation β_S . In other words, our previous model in [9] still works effectively when a partial fingerprint covers a sufficiently large portion of the original full print.

In this paper, it is our interest to investigate situations where it is not possible to omit β_{χ} - either because the size of χ is not negligible or the unavailable area conceals critical information. To reach that end, we first establish the general solution space for (5) such that data fidelity can be governed in the known region Ω when estimating β_S .

3.2 General Solution Space

For any real matrix $\Psi \in \mathbb{R}^{M \times K}$, there exist unitary matrices $\mathbf{U} \in \mathbb{R}^{M \times M}$ and $\mathbf{V} \in \mathbb{R}^{K \times K}$ and a diagonal matrix $\Lambda \in \mathbb{R}^{M \times K}$ with nonnegative diagonal elements, such that [22]

$$\Psi = \mathbf{U} \Lambda \mathbf{V}^T. \quad (6)$$

By appropriate permutation, the diagonal elements of Λ can be arranged in a non-increasing order: $\lambda_1 \geq \lambda_2 \geq \dots \geq \lambda_{\min(M, K)}$.

The factorization (6) is called *singular value decomposition* (SVD) of Ψ . Note that $\mathbf{U}^T \mathbf{U} = \mathbf{U} \mathbf{U}^T = \mathbf{I}(M \times M)$ and $\mathbf{V}^T \mathbf{V} = \mathbf{V} \mathbf{V}^T = \mathbf{I}(K \times K)$, where \mathbf{I} is an identity matrix. The columns of \mathbf{U} and \mathbf{V} are called singular vectors of Ψ , and the diagonal elements in Λ are singular values associated with the corresponding singular vectors.

By SVD truncation [22], i.e. zeroing singular values that are below the cutoff threshold ϵ , one controls the span of the singular vectors, and thus effectively damps the least square solution of a linear system $\mathbf{y} = \Psi \mathbf{x}$. That is,

$$\Psi = [\mathbf{U}_r \quad \mathbf{U}_n] \begin{bmatrix} \Lambda_r & 0 \\ 0 & \Lambda_n \end{bmatrix} \begin{bmatrix} \mathbf{V}_r^T \\ \mathbf{V}_n^T \end{bmatrix} \approx \mathbf{U}_r \Lambda_r \mathbf{V}_r^T. \quad (7)$$

In this way, \mathbf{U} and \mathbf{V} are partitioned simultaneously. The lower singular values in Λ_n are zeroed. The matrix Ψ can be approximately represented by the most significant components in SVD. The pseudo inverse of Ψ is thus $\Psi^\dagger = \mathbf{V}_r \Lambda_r^{-1} \mathbf{U}_r^T$.

The *null space* of a data set, such as Ψ , is defined as the kernel whose elements can be mapped to zero by Ψ [23]. That is,

$$\mathcal{N}(\Psi) = \{\mathbf{b} \in \mathbb{R}^{K \times 1} | \Psi \mathbf{b} = 0\}. \quad (8)$$

For an arbitrary vector $\alpha \in \mathbb{R}^{n \times 1}$, where n is the number of singular vectors to be eliminated, it is easy to prove that $\mathbf{b} = \mathbf{V}_n \alpha$ projects α into the null space of Ψ , noting that the singular vectors \mathbf{V}_r and \mathbf{V}_n are orthogonal to each other.

According to (8), any change made in the null space will not affect the result of $\mathbf{y} = \Psi \mathbf{x}$, since $\mathbf{y} = \Psi(\mathbf{x} + \mathbf{b}) = \Psi \mathbf{x} + \Psi \mathbf{b} = \Psi \mathbf{x}$. Therefore, $(\mathbf{x} + \mathbf{b})$ is another solution that yields the same \mathbf{y} as solution \mathbf{x} . The *null space shuttles* [24] then refers to the operator that moves from one solution to another in the solution space through projection in the null space of the system matrix Ψ .

We propose to adopt the concept of null space shuttles for exploring all possible solutions of (5) while preserving best-fit of the existing data in the least square sense. Without loss of generality, assume M phase samples \mathbf{d}_Ω in the partial fingerprint segment $\Omega \subset S$. Rewrite (1) in matrix notation. Accordingly, the phase data in Ω can be reconstructed by

$$\hat{\mathbf{d}}_\Omega = \Psi_\Omega \beta_S, \quad (9)$$

where Ψ_Ω is an $M \times K$ matrix with $K = (2k + 1)^2$ being the number of basis functions:

$$\Psi_\Omega = [\Psi(x_1, y_1) \quad \Psi(x_2, y_2) \quad \dots \quad \Psi(x_M, y_M)]^T \quad (10)$$

where $\Psi(x, y) = \{\psi_{ij}(x, y) | i, j = 0, 1, \dots, 2k\}$ and $\psi_{ij}(x, y) = p_i(x) \cdot q_j(y)$ with

$$p_i(x) = \begin{cases} 1/2 & (i = 0) \\ \cos m\nu x & (i = 2m - 1, m = 1, 2, \dots, k) \\ \sin m\nu x & (i = 2m, m = 1, 2, \dots, k) \end{cases}$$

and

$$q_j(y) = \begin{cases} 1/2 & (j = 0) \\ \cos n\omega y & (j = 2n - 1, n = 1, 2, \dots, k) \\ \sin n\omega y & (j = 2n, n = 1, 2, \dots, k) \end{cases}$$

where ν and ω are fundamental frequencies defined in [9]. It is worth to note that $\Psi(x, y)$ is a bilinear function of $p_i(x)$ and $q_j(y)$. This relation is beneficial for deriving the partial derivative forms of $\Psi(x, y)$ by taking the partial derivatives of $p_i(x)$ and $q_j(y)$ respectively, which will be shown later in Section 4.1.

Taking SVD over Ψ_Ω , the set of all least square solutions to (9) is then governed by

$$\beta_S = \Psi_\Omega^\dagger \mathbf{d}_\Omega + \mathcal{N}(\Psi_\Omega) = \mathbf{V}_r \Lambda_r^{-1} \mathbf{U}_r^T \mathbf{d}_\Omega + \mathbf{V}_n \alpha, \quad (11)$$

where α is an arbitrary vector. It can be proved that all solutions defined by (11) preserve data fidelity in the

existing segment Ω since

$$\begin{aligned} \hat{\mathbf{d}}_\Omega &= \Psi_\Omega \beta_S \approx \Psi_\Omega \mathbf{V}_r \Lambda_r^{-1} \mathbf{U}_r^T \mathbf{d}_\Omega + \Psi_\Omega \mathbf{V}_n \alpha \\ &= (\mathbf{U}_r \Lambda_r \mathbf{V}_r^T \mathbf{V}_r \Lambda_r^{-1} \mathbf{U}_r^T) \times \mathbf{d}_\Omega + (\mathbf{U}_r \Lambda_r \mathbf{V}_r^T \mathbf{V}_n) \times \alpha \\ &= \mathbf{d}_\Omega. \end{aligned} \quad (12)$$

Note that \mathbf{V}_r and \mathbf{V}_n are orthogonal.

Therefore, we use (11) to define the *general solution space* for evaluating the global model representation β_S , given an existing segment $\Omega \subset S$, such that data fidelity in Ω can be preserved in the sense of least square fitting errors.

On the other hand, estimates in the unknown region, $\hat{\mathbf{d}}_\chi$, will be affected by both input phase samples \mathbf{d}_Ω and the choice of α . The proof is as follows. Since $\hat{\mathbf{d}}_\chi = \Psi_\chi \beta_S$, where Ψ_χ is a $N \times K$ matrix with N being the number of points in χ and $K = (2k + 1)^2$ being the number of basis functions, similar to (12), we have

$$\begin{aligned} \hat{\mathbf{d}}_\chi &= \Psi_\chi \Psi_\Omega^\dagger \mathbf{d}_\Omega + \Psi_\chi \mathbf{V}_n \alpha \\ &= (\Psi_\chi \mathbf{V}_r \Lambda_r^{-1} \mathbf{U}_r^T) \times \mathbf{d}_\Omega + (\Psi_\chi \mathbf{V}_n) \times \alpha. \end{aligned} \quad (13)$$

Because Ψ_χ is not related to Ψ_Ω , neither the term $(\Psi_\chi \mathbf{V}_r \Lambda_r^{-1} \mathbf{U}_r^T)$ nor the term $(\Psi_\chi \mathbf{V}_n)$ can be eliminated. Therefore, $\hat{\mathbf{d}}_\chi$ is affected by both terms in (13), i.e. the existing data samples \mathbf{d}_Ω and the null space vector α .

There are also some remarks regarding the SVD process. When the cutoff threshold ϵ of SVD truncation is set to zero, the null space vector is not included in the solution. Therefore, $\beta_S = \Psi_\Omega^\dagger \mathbf{d}_\Omega$ yields exactly the same solution as that from (3) or the linear least square algorithm [9].

When the value of the cutoff threshold ϵ increases, more singular values are eliminated from the pseudo inverse. Accordingly, more singular vectors will be added to \mathbf{V}_n . As a result, the null space vectors will impose more impact on data estimation in the unknown region χ but at a cost of data fitting in the known region Ω .

4 RECONSTRUCTION ALGORITHMS

In the previous section, we establish (11) to yield the general solution space for estimating the global orientation feature representation from incomplete samples in the partial fingerprint segments. To further damp the solution space, we require more knowledge to evaluate the null space vector α . Fortunately, fingerprint ridge topology patterns are not random images. They in general possess some intrinsic features as we have discussed in Section 2. These a priori knowledge will be useful for ridge topology reconstruction.

From (4) and (5), we know that the global representation β_S can be evaluated if phase data in the unknown region \mathbf{d}_χ can be somehow estimated. In the following, we propose two reconstruction algorithms for estimating \mathbf{d}_χ by taking into account the a priori knowledge of ridge smoothness and peripheral arches, respectively.

4.1 Smooth Extensions

Without loss of generality, we consider partial fingerprint segment Ω in a defined 2D image site S . Assuming good continuation of ridge flows, we wish to prolong flow trends arriving at the boundaries of Ω smoothly into the unknown region χ . In Section 3.2, (13) indicates that estimates $\hat{\mathbf{d}}_\chi$ must contain information from the existing segment Ω . This hints that the structure information in Ω should be propagated progressively into the unknown region χ .

We denote Δ as a thin band encompassing the known segment $\Omega^{(0)}$, and $\Omega^{(1)} = \Omega^{(0)} \cup \Delta$ as the combined region after expansion. From (1), we know that the phase estimates

$$\hat{d}(x, y) = \Psi(x, y)\beta^{(1)}, \quad \forall (x, y) \in \Omega^{(1)} \quad (14)$$

where $\beta^{(1)}$ is the model coefficient vector evaluated in the local region $\Omega^{(1)}$. In other words, $\beta^{(1)}$ can be regarded as a function, denoted $\mathbf{g}(\Omega^{(1)})$, of the phase structures in $\Omega^{(1)}$. Thus, by taking the Taylor's expansion of $\beta^{(1)}$ at the known segment $\Omega^{(0)}$, we have

$$\beta^{(1)} = \mathbf{g}(\Omega^{(1)}) = \mathbf{g}(\Omega^{(0)}) + \mathbf{g}'(\Omega^{(0)})\Delta + \mathcal{O}(\Delta), \quad (15)$$

where \mathbf{g}' is the derivative function and $\mathcal{O}(\Delta)$ is the residue. Note that $\Delta = \Omega^{(1)} - \Omega^{(0)}$ is the expanded area. When Δ is arbitrarily small, i.e., $\Delta \rightarrow 0$, both the second term and the residue on the right hand side of (15) become negligible. Therefore, $\beta^{(1)}$ can be approximated by $\beta^{(0)} = \mathbf{g}(\Omega^{(0)})$. By substituting it into (14) and noting that $\Delta \subset \Omega^{(1)}$, we have

$$\hat{d}(x, y) = \Psi(x, y)\beta^{(0)}, \quad \forall (x, y) \in \Delta. \quad (16)$$

Algorithm 1 Smooth Extensions

SMEXT(Ω , $\mathbf{d}_{\Omega, \text{cos}}$, $\mathbf{d}_{\Omega, \text{sin}}$)

- 1 Initialize $k \leftarrow 0$;
- 2 $\Omega^{(0)} \leftarrow \Omega$ and $\beta_l^{(0)} \leftarrow \tilde{\Psi}_\Omega^T \mathbf{d}_{\Omega, l}$ ($l = \text{cos}, \text{sin}$);
- 3 While $(S - \Omega^{(k)}) \neq \emptyset$
- 4 **do**
- 5 Let $\Omega^{(k+1)} \leftarrow \text{Dilate } \Omega^{(k)}$,
- 6 Let $\Delta \leftarrow \Omega^{(k+1)} - \Omega^{(k)}$,
- 7 Evaluate $\hat{\mathbf{d}}_{\Delta, l} = \Psi_\Delta \beta_l^{(k)}$ ($l = \text{cos}, \text{sin}$),
- 8 NORMALIZE($\hat{\mathbf{d}}_{\Delta, \text{cos}}, \hat{\mathbf{d}}_{\Delta, \text{sin}}$),
- 9 Update $\beta_l^{(k+1)} \leftarrow \beta_l^{(k)} + \tilde{\Psi}_\Delta^T \hat{\mathbf{d}}_{\Delta, l}$
- 10 Let $\Omega^{(k+1)} \leftarrow \Omega^{(k)}$ and $k \leftarrow k + 1$;
- 11 Evaluate $\hat{\mathbf{d}}_{\chi, l} = \Psi_\chi \beta_l^{(k)}$ ($l = \text{cos}, \text{sin}$);
- 12 Output NORMALIZE($\hat{\mathbf{d}}_{\chi, \text{cos}}, \hat{\mathbf{d}}_{\chi, \text{sin}}$).

NORMALIZE($\mathbf{d}_{\text{cos}}, \mathbf{d}_{\text{sin}}$)

- 1 Let $\Theta \leftarrow \arctan(\mathbf{d}_{\text{sin}}, \mathbf{d}_{\text{cos}})$
 - 2 Output $\mathbf{d}_{\text{cos}} \leftarrow \cos(\Theta)$ and $\mathbf{d}_{\text{sin}} \leftarrow \sin(\Theta)$.
-

Written in matrix notation, (16) is equivalent to $\hat{d}_\Delta(x, y) = \Psi_\Delta \beta^{(0)}$. By this way, the structure information in the known segment $\Omega^{(0)}$ is conveyed into the surrounding band Δ . Note that the basis function $\Psi(x, y)$ is readily evaluated at every point in the phase plane, regardless of the position. Therefore, it is independent of the phase structure information in $\Omega^{(1)}$.

It is necessary to emphasize that the approximation in (16) is subject to the condition that the expanding region Δ is *small*. To expand the area further into the unknown region χ , we must update the phase structure in the new available segment $\Omega^{(k+1)}$ upon last expansion. That is,

$$\beta^{(k+1)} = \beta^{(k)} + \tilde{\Psi}_\Delta^T \hat{\mathbf{d}}_\Delta, \quad k = 0, 1, 2, \dots, t-1. \quad (17)$$

By iterating the above process, say after $t-1$ times,

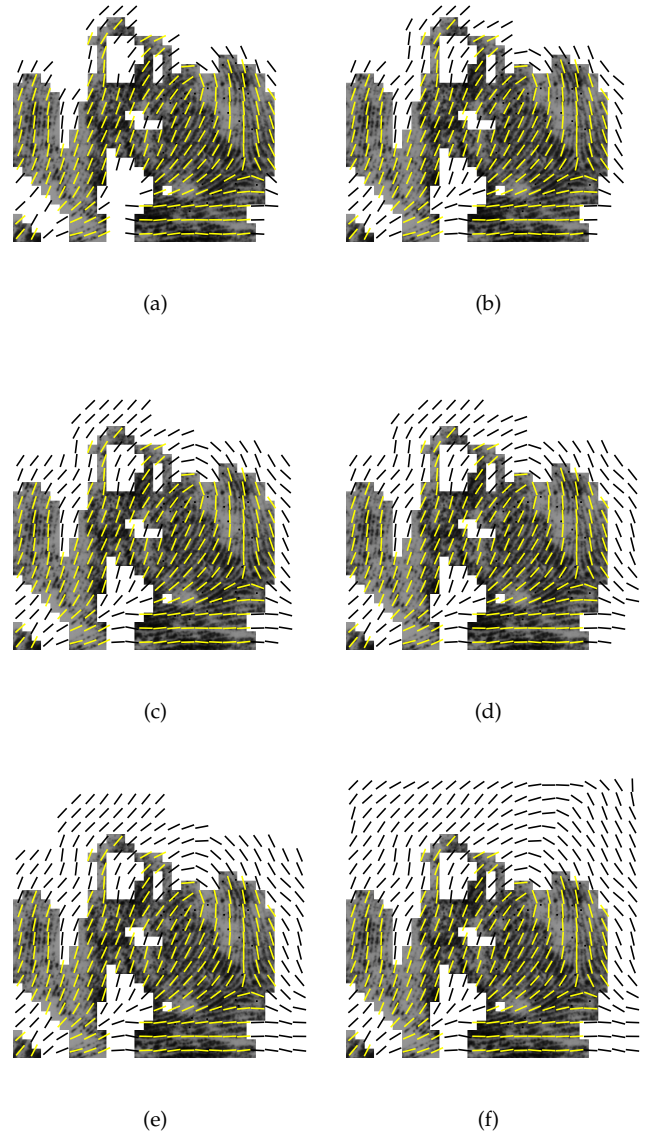


Fig. 3. Smooth Extensions for reconstruction with singular points.

the unknown region χ is filled with phase estimates. We name the algorithm *Smooth Extensions* since the expansion process is based on the a priori knowledge of ridge smoothness and continuity. Algorithm 1 outlines the main procedure.

Note that in Algorithm 1, there is a subroutine normalizing the numerical vectors \mathbf{d}_{\cos} and \mathbf{d}_{\sin} to produce cosine and sine phases through the corresponding orientation angles Θ . This is to ensure the constraint that the squared sum of cosine and sine components equals to one at each point in the phase plane.

Figure 3 illustrates expansion process for the latent fingerprint example displayed in Fig. 1(a). Note that the background and the obscure regions are removed from the original image, resulting in partial fingerprint

segments shown in Fig. 3. The example demonstrates how ridge orientation estimation is expanding into the unknown regions. Due to space limit, we only display a few intermediate stages of the “growing” process.

Figures 4 demonstrates another example using the Smooth Extensions algorithm for reconstructing ridge orientation patterns. The partial fingerprint also has the background and contaminated areas removed. Note that in the partial fingerprint image, the central part that contains critical information of singular points is missing.

Figures 3 and 4 illustrate two representative scenarios for which Smooth Extensions can be adopted: 1) with critical information of singular points and 2) with peripheral ridge samples. It is easy to understand the first scenario since ridge patterns are generally smooth except where singularity is present as shown in Fig. 3. For the second scenario, we demonstrate in Fig. 4 that it is possible to induce singularity from its peripheral trends. This is because singular points are type of control points around which ridge flows are “wrapped” [7]. Therefore, the peripheral patterns actually imply information of the internal singularity patterns.

To further demonstrate the second scenario, Fig. 5 shows an example of using Smooth Extensions to reconstruct the global topology pattern from minutiae triplets. In this case, minutiae triplets are regarded as discrete yet globally distributed ridge samples. The reconstruction result, shown on the right, closely resembles the original fingerprint image on the left.

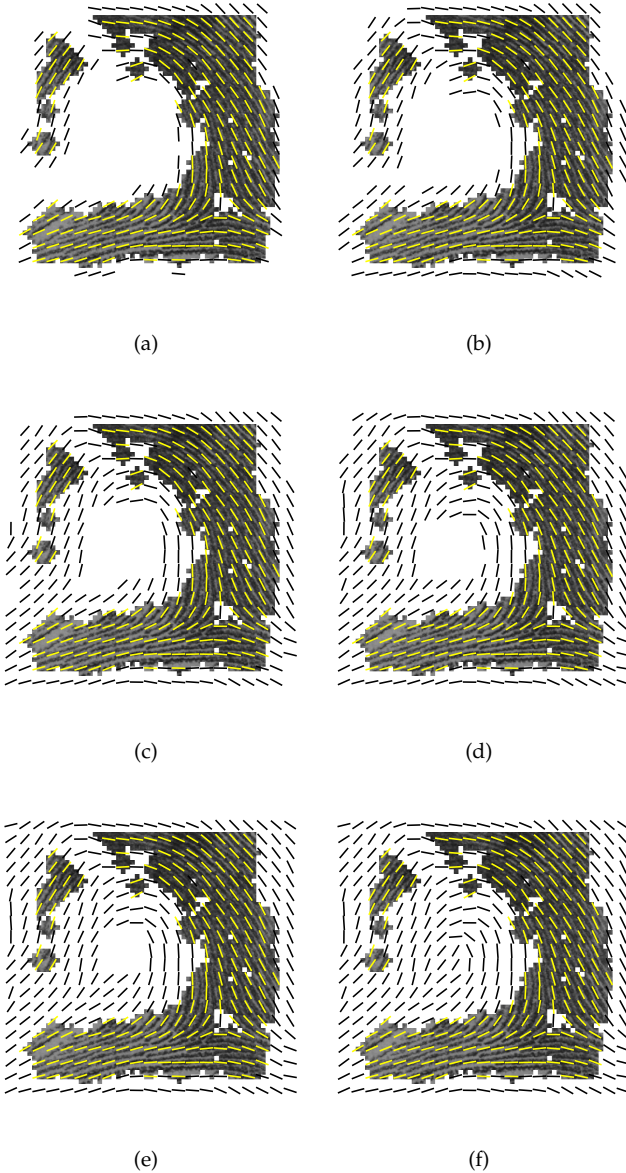


Fig. 4. Smooth Extensions for reconstruction with peripheral samples.

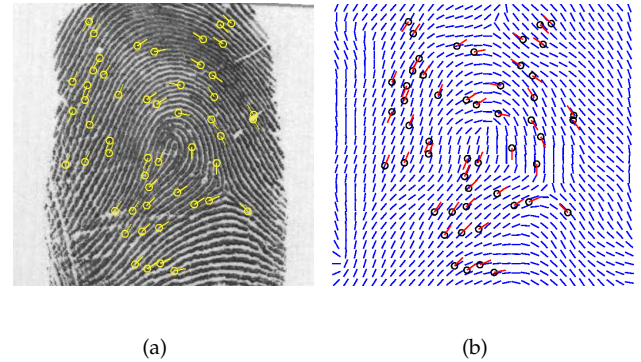


Fig. 5. Reconstruction from minutiae triplets

Note that some partial fingerprints can lose one or more critical singular points and the available ridge samples are all concentrated in local areas, i.e. the amount of global information is insufficient. In such cases, using the Smooth Extensions algorithm alone cannot induce the missing singularity patterns after reconstruction. To resolve this problem, we shall further incorporate the other a priori knowledge of peripheral arches.

4.2 Modeling Peripheral Arches

In Section 2, we have shown that ridge flows in the outer peripheral regions of fingerprints generally exhibit some

arch forms. In cases where the peripheral ridge samples are not available in the partial fingerprint segments, it is necessary to introduce the a priori knowledge of peripheral arches into the estimation process. In this section, we propose a model-based approach for generating peripheral arches based on existing partial fingerprint segments. Specifically, we investigate two mathematical models.

4.2.1 Cosine peripheral model

We first consider the conditional cosine model that has been used in fingerprint synthesis for the arch-typed fingerprints [7], [25]. We slightly modify the conditional cosine model [25] by introducing an additional control parameter as follows:

$$\phi(x, y) = \arctan(\max\{0, k_1 - k_2 \cdot \frac{y+l}{2l}\} \cdot \cos(\frac{x+h}{2h}\pi)) , \quad (18)$$

where $(x, y) \in S : (-l \leq x \leq l, -h \leq y \leq h)$ and k_1 and k_2 are the control parameters. Figure 6 plots a group of arch forms generated by (18) with different parameters. Note that k_1 contributes to curvature changes of the arches, and k_2 determines the lifting level of bottom lines.

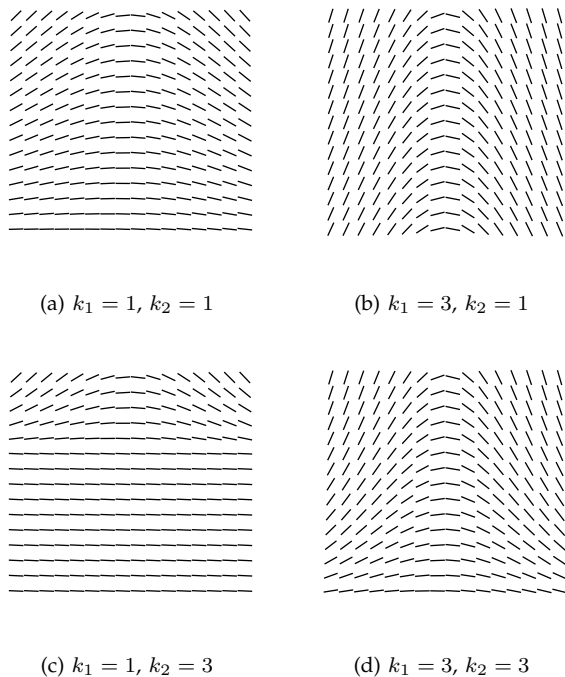


Fig. 6. Arch forms generated using the conditional cosine model with various parameters.

The conditional cosine functions were initially designed for modeling arch-typed fingerprints in the full plane. Therefore, the model does not consider possible inclusion of any internal singularity pattern. However, since ridge flows are “wrapped” around singular points,

an internal singularity pattern actually affect the formation and shape of the outer peripheral trends. Intuitively, we consider a mathematical model that can inherently interpret this strong link will be more suitable for describing the fingerprint peripheral arches.

4.2.2 Fluid peripheral model

The above consideration leads to our second peripheral model originated from fluid dynamics. The streaming functions have been initially studied for describing fluid motions in the discipline of theoretical hydrodynamics [26]. We are motivated to use the streaming functions in this context due to the close resemblance between the fingerprint peripheral arches and the flow patterns of streaming fluids when they proceed through a circular cylinder.

The fluid model inherently implies existence of internal singularities. In particular, the core point of a concentric cylinder is the center of circulation that affects the shape of rounding flows, and deltas can be naturally created when the embedded circulating cylinder divides the streamlines. Therefore, we believe that the streaming functions are more suitable for modeling the peripheral arches of fingerprints. In the following, we demonstrate how it can be adapted for this purpose.

Mathematically, the fluid model considers two dimensional flow of incompressible fluid in a complex plane z . The streamlines compose a stable pattern when the motion is steady. Assume a uniform stream advancing towards a concentric cylinder $|z| = a$ in a unit speed along the x -axis. The complex potential of the stream is therefore z . If the cylinder is running with a circulation strength of $\kappa \in \mathbb{R}$, i.e. the speed at unit distance from the origin, then the complex potential of the stream becomes [26]:

$$\omega = (z + \frac{a^2}{z}) + i\kappa \lg \frac{z}{a} . \quad (19)$$

The first part on the right hand side of (19) represents the streaming motion and the second part represents the circulation motion.

By differentiating the complex potential with respect to z , we have

$$\frac{d\omega}{dz} = 1 - \frac{a^2}{z^2} + i\frac{\kappa}{z} . \quad (20)$$

Since the complex velocity of the stream is defined as $u - iv = -(d\omega/dz)$, the instant velocity components in the cartesian coordinates are

$$\begin{aligned} u &= -1 + \frac{a^2}{r^4} \cdot (x^2 - y^2) - \kappa \frac{y}{r^2} \\ v &= -\frac{a^2}{r^4} \cdot 2xy + \kappa \frac{x}{r^2} , \end{aligned} \quad (21)$$

where $r^2 = x^2 + y^2$. The angular argument of the complex velocity indicates the instant tangential direction on the streamline. Accordingly,

$$\phi(x, y) = \arctan \left(\frac{v(x, y)}{u(x, y)} \right) \quad (22)$$

plots the phase portrait of flow pattern once the velocity vector (u, v) at every point $z = (x, y)$ is derived in the field.

Figure 7 plots a group of flow patterns generated by (21) with different parameters. It clearly shows that the peripheral patterns outside the cylinder change significantly with parameter a and κ . This is because the contour of the cylinder must form part of the streamlines, and the general effect of circulation is to increase the speed of the fluids at points above the cylinder while diminishing the speed at points below. Therefore, increasing the circulation strength κ increases the curvature of the peripheral arches. According to our empirical experience, defining κ in the range of $[a, 2a]$ is able to yield a reasonable shape of peripheral arches for partial fingerprint segments.

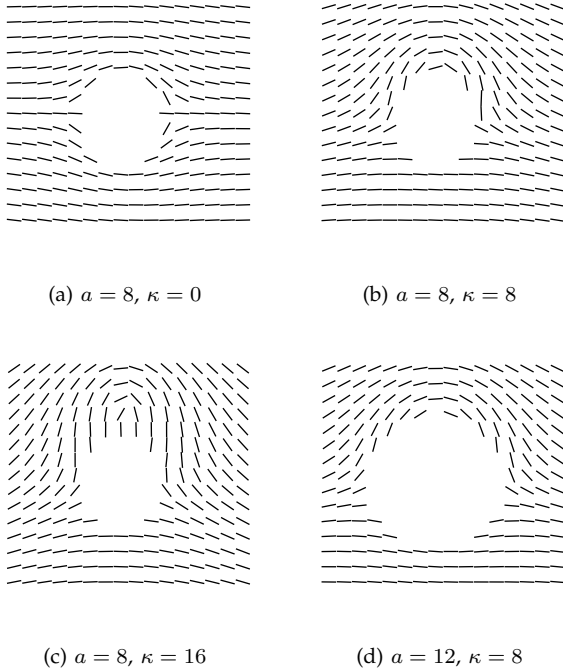


Fig. 7. Flow patterns assuming a circular cylinder $|z| = a$ with circulation strength κ in uniform streams.

For robustness, we also introduce two more parameters (dx, dy) for offsetting x and y from the center coordinates. This allows us to translate the circular cylinder to any position in the plane. Accordingly, the fluid model (21) is simply modified by replacing the x and y in (21) with new coordinates $(x + dx)$ and $(y + dy)$.

4.2.3 Incorporating peripheral arches

The problem now boils down to parameter evaluation of our modeling approach. Since there is no ground truth available in the peripheral region, we propose to train the peripheral model with initial estimates obtained by Smooth Extensions over the existing partial fingerprint segments. Then, we combine orientation samples in the

known region with estimates in the model-generated peripheral arches to reconstruct the overall ridge topology pattern. Algorithm 2 describes the main procedure.

Algorithm 2 Incorporating Peripheral Arches

PERARCH($\Omega, \mathbf{d}_{\Omega, \cos}, \mathbf{d}_{\Omega, \sin}$)

- 1 Partition χ into χ_I and χ_{II} ;
- 2 Initialize $(\hat{\mathbf{d}}_{\chi, \cos}, \hat{\mathbf{d}}_{\chi, \sin})$ by *SmoothExt*($\Omega, \mathbf{d}_{\Omega, \cos}, \mathbf{d}_{\Omega, \sin}$);
- 3 Get $\{\hat{\theta}(x, y) | (x, y) \in \chi_I\} \leftarrow \arctan(\hat{\mathbf{d}}_{\chi_I, \sin}, \hat{\mathbf{d}}_{\chi_I, \cos})$;
- 4 Find $P^* = \arg \min_P f_{\text{cost}}(P; \hat{\theta})$;
- 5 $\hat{\Phi}_{\chi_I} \leftarrow \{\hat{\phi}(x, y; P^*) | (x, y) \in \chi_I\}$;
- 6 $\hat{\mathbf{d}}_{\chi_I, \cos} \leftarrow \cos(\hat{\Phi}_{\chi_I}), \hat{\mathbf{d}}_{\chi_I, \sin} \leftarrow \sin(\hat{\Phi}_{\chi_I})$;
- 7 $\Omega' \leftarrow (\Omega \cup \chi_I), \mathbf{d}_{\Omega', l} \leftarrow \{\mathbf{d}_{\Omega, l}, \hat{\mathbf{d}}_{\chi_I, l}\} \quad (l = \cos, \sin)$;
- 8 $(\hat{\mathbf{d}}_{\chi_{II}, \cos}, \hat{\mathbf{d}}_{\chi_{II}, \sin}) \leftarrow \text{SmoothExt}(\Omega', \mathbf{d}_{\Omega', \cos}, \mathbf{d}_{\Omega', \sin})$;
- 9 Output $\hat{\mathbf{d}}_{\chi, l} \leftarrow \{\hat{\mathbf{d}}_{\chi_I, l}, \hat{\mathbf{d}}_{\chi_{II}, l}\} \quad (l = \cos, \sin)$

We first partition the unknown region χ into two parts, namely χ_I and χ_{II} . Subsection χ_I is governed by the peripheral model, either the cosine peripheral or the fluid peripheral, while subsection χ_{II} is the transition region that connects χ_I and the existing segment Ω via Smooth Extensions. In practice, we perform the partition with a circular window, e.g. tangential to the site S , to define χ_I as the peripheral corners outside the circular window and χ_{II} as the remaining area between χ_I and Ω . We obtain the initial phase estimates $(\hat{\mathbf{d}}_{\chi, \cos}, \hat{\mathbf{d}}_{\chi, \sin})$ via Smooth Extensions over the existing partial fingerprint segments. Wherever Ω overlaps with χ_I , \mathbf{d}_{Ω} are used in preference.

Denote the parameter set of a peripheral model as P . In case of cosine peripheral, $P = \{k_1, k_2\}$ where k_1 and k_2 are control parameters of the conditional cosine functions. In case of fluid peripheral, $P = \{a, \kappa, dx, dy\}$ where a is the cylinder radius, κ is the circulation strength, dx and dy are coordinate offsets of the cylinder center. We propose to evaluate P by minimizing the following cost function:

$$f_{\text{cost}}(P; \hat{\theta}) = \sum_{(x, y) \in \chi_I} \sin^2(\hat{\phi}(x, y) - \hat{\theta}(x, y; P)), \quad (23)$$

where both $\hat{\theta}$ and $\hat{\phi}$ are orientation angles in π periodic. The cost function (23) maps orientation difference into a continuous range of $[0, 1]$. The efficacy of this distance measure between orientation angles can be found in [27]. Note that by using the $\sin^2(\cdot)$ function we obtain the same distance measure regardless of the sign of $(\hat{\phi} - \hat{\theta})$. When $(\hat{\phi} - \hat{\theta})$ equals to 0 or $\pm\pi$, i.e. parallel orientations, the distance measure $\sin^2(\cdot)$ has the minimum value of zero. When the orientation difference equals to $\pm\pi/2$, i.e. orthogonal orientations, $\sin^2(\cdot)$ reaches the maximum value of one.

By minimizing the cost function (23), we are able to evaluate the optimal parameter set P^* of a peripheral

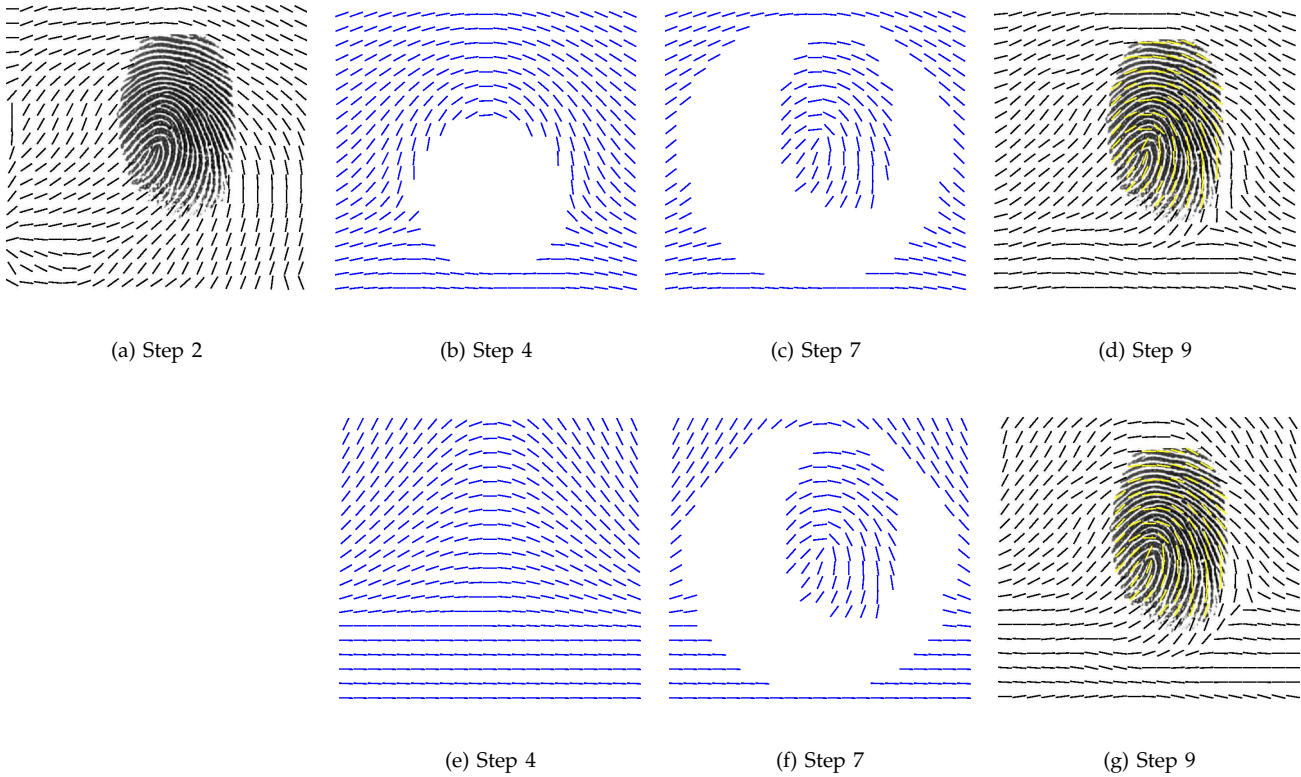


Fig. 8. Plots (a), (b), (c) and (d) demonstrate Algorithm 2 incorporating the fluid peripheral model. Plots (a), (e), (f) and (g) demonstrate Algorithm 2 incorporating the cosine peripheral model.

model to minimize the total orientation differences between the initial estimates $\hat{\theta}$ and the model estimates $\hat{\phi}$ in the subregion χ_I . In our implementation, the optimization is performed by the Matlab minimization routine *fmincon*. Figure 8 demonstrates main steps of Algorithm 2 incorporating the fluid peripheral model.

As shown in Fig. 8(a), Smooth Extensions is applied first to produce the initial estimates in the overall unknown region χ . It can be observed that, although upper trends above the core are well estimated the due delta pattern is still missing in the bottom right area.

Figure 8(b) plots the output of Step 4 in Algorithm 2 incorporating the fluid peripheral (21). The phase portrait is generated by the optimal parameter set through minimizing the cost function (23). Figure 8(c) plots input to the secondary expansion in which the peripheral arches are combined with existing data in the partial fingerprint segment for evaluating trends in the transition region χ_{II} . Figure 8(d) displays the final estimation result. Note that the delta pattern emerges in the expected area.

For comparison, figures 8(e)-8(g) plot the corresponding procedure when incorporating the cosine peripheral in Algorithm 2. For the result, we use the same initial estimates in Fig. 8(a) to train the conditional cosine functions (18). Comparing Fig. 8(d) and Fig. 8(g), it can be observed that although both methods are able to reconstruct a delta pattern, the fluid peripheral method

is more adaptive to the existing segment and thus the global topology pattern is more naturally rounded around the existing pattern. The reconstruction results also show that, by fitting data in the existing regions alone, there can be more than one valid solutions.

Figure 9 demonstrates another example of orientation reconstruction. Figure 9(a) is the original full print. We test our algorithms using data samples only in the delta regions shown in the subsequent figures to reconstruct the global ridge orientation pattern. Note that in the partial fingerprint, the critical core structures are missing and no peripheral information is available. Figure 9(b) plots the reconstruction result by applying a 2D Gaussian filter to the original FOMFE estimates, with window size $w = 40 \times 40$ and the smoothing parameter $\sigma = 5$. It can be seen that the 2D Gaussian filter does not produce constructive estimates in the blank regions.

Figures 9(c) and 9(d) plot reconstruction results from the segmented delta patterns using the cosine peripheral and the fluid peripheral, respectively. Comparing with Fig. 9(b), it is clear that when the a priori knowledge of peripheral arches is introduced the estimation can be significantly improved. Comparing the two, however, Fig. 9(d) resembles the original full print more closely especially in the outer peripheral arch region. This is because the fluid model inherently considers the existence of singularity, and thus is able to round the peripheral flows accordingly.

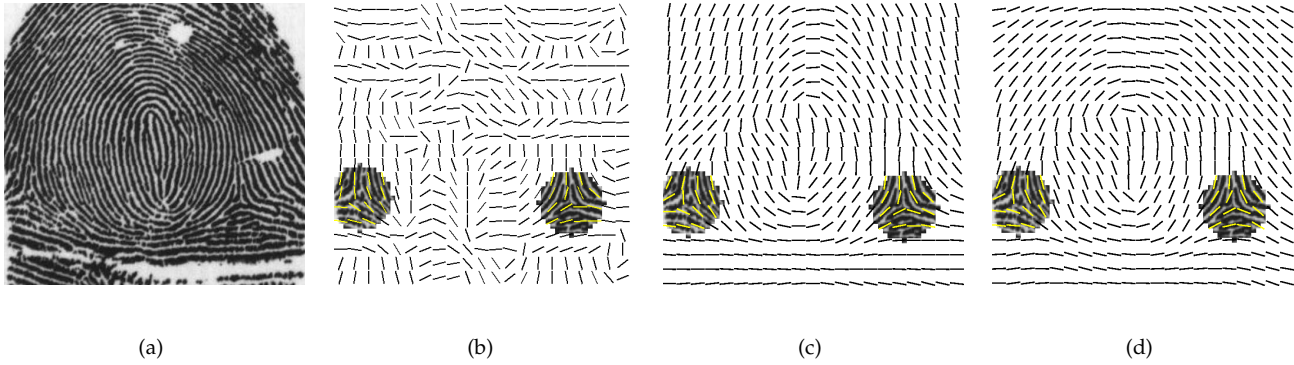


Fig. 9. Reconstruction of original fingerprint image in (a) from Algorithm 2 using: (b) 2D Gaussian filter with $w = 20, \sigma = 5$, (c) the cosine peripheral, (d) the fluid peripheral.

Nevertheless, the fluid model in (21) can be further improved. For instance, (19) only considers streams flowing in the horizontal direction. The resulting peripheral arches are thus leveled. If the internal partial fingerprints are not leveled instead, erratic patterns may be generated when connecting the peripheral arches with the internal segments. To solve the problem, one possible improvement is to adjust the streaming direction in consistency with the orientation of the partial segments. However, it is beyond the scope of this paper and will be investigated in our future work.

5 STATISTICAL EXPERIMENTS

This section evaluates the performance of our proposed algorithms via statistical experiments. Section 5.1 assesses the orientation estimation accuracy. The test segments used in this test mimic cases, such as some latent prints, in which the critical singularities are included and the partial segments are randomly located in different parts of the original full prints. Section 5.2 investigates the quality of partial fingerprints from a new perspective, which is followed by Section 5.3 that uses groups of partial fingerprints of controlled quality to evaluate the fingerprint retrieval performance using the proposed orientation reconstruction methods.

5.1 Orientation Estimation Accuracy

The NIST special database 14 (SDB) [29] consists of rolled prints scanned from fingerprint cards. Among the records, a significant portion is full prints (i.e. rolled from nail to nail and from tip to the joint). The scanned resolution is $500dpi$ and the fingerprint image size is 480×512 pixels after segmentation. There are two impressions recorded for each instance, namely the F prints and S prints. We first randomly select 100 S prints that are full prints, and compute the ridge orientations as in [9]. One example is displayed in Fig. 10(a). We also superimposed ridge orientation field and marked singular points with ‘ \circ ’ and ‘ \triangle ’ on the image.

For each test subject, we perform a routine of fingerprint image quality assessment from the NFIS2 software [6], and obtain a quality map marking reliability of local fingerprint image areas at five levels. We extract an image foreground with the highest quality level and produce a partial fingerprint segment by image erosion on that foreground to remove random bits. Figure 10 shows a typical example of such partial fingerprints generated in the test. In this way, we can simulate the situation of latent fingerprints in which the available partial segments are randomly located in different parts of the original full print. This is because the image quality of a fingerprint varies from one to another. Hence, the location and the shape of segmentation are both random. Moreover, the NFIS2 quality assessment routine regards high curvature areas, which are often presented in singularity regions, as being more difficult for orientation estimation, and thus tends to assign lower quality scores to those regions for the estimation results can be less reliable. Therefore, partial fingerprints generated in this test do not contain any singularity, and even singularity regions are usually removed after the image erosion process.

Fortunately, peripheral ridge samples are generally available for the test segments. Therefore, it is suitable to use our Smooth Extensions method proposed in Section 4.1 for reconstructing removed parts of the ridge orientation structure. For the purpose of comparison, we have also implemented other interpolation techniques to perform the same task. In particular, we use the ridge orientation interpolation method based on the constrained Delaunay triangulation (CDT) as introduced in [28], except that segmentation is performed through the NFIS2 quality assessment routine instead of setting a threshold on the coherence measures. Data sites for interpolation are composed of points on the contours of segmentation and those at four corners of the image bounding box. The contour lines are regarded as constraints of predefined edges. Figure 10(b) shows the resulting CDT construction. The gray area marks the

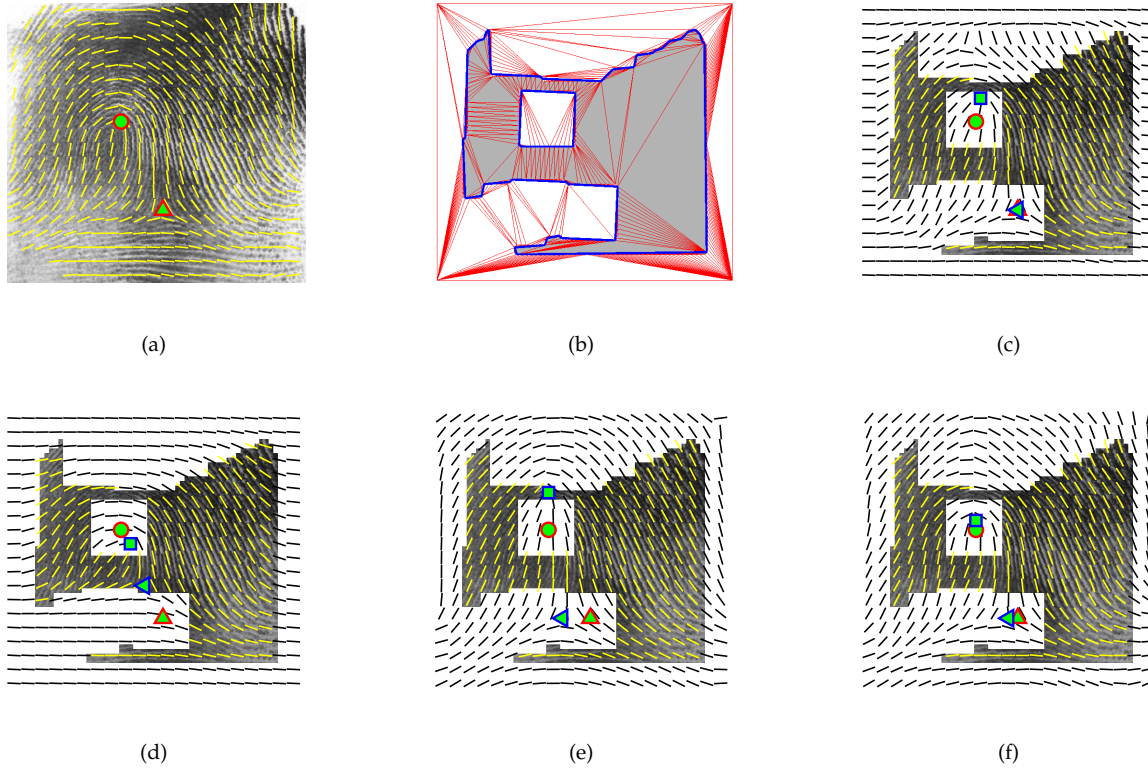


Fig. 10. Testing orientation estimation accuracy: (a) original full print, with singular point detections (marked by 'O' and 'Δ'); (b) constrained Delaunay triangulation (CDT): data points on the segmentation contour and at four corners, and predefined edges (constraints) on the contour segments; (c) linear interpolation from the CDT construction in (b) [28], (d) Gaussian smoothing over orientations values estimated from FOMFE in the foreground, assuming zeroes in the non-foreground, with $w = 40 \times 40$, $\sigma = 5$; (e) Gaussian smoothing over orientation values estimated from FOMFE in the overall area [9], with $w = 40 \times 40$ and $\sigma = 10$; (f) Smooth Extensions. (the estimated singular points are marked by '□' and '◁' in the above figures).

partial fingerprint segment generated for this example. The contour lines are highlighted. The remaining blank region is the area to be estimated. Orientation values of points on the contours are estimated by evaluating FOMFE over the partial fingerprint area, and zero orientations are assigned to the four corner points of the bounding box. Then, linear triangular interpolation [30] is performed to estimate orientation values for points in the unknown region from those in data sites. The FOMFE estimates are retained for points in the gray foreground area. The combined result is plotted in Fig. 10(c).

We note that the CDT based interpolation method works reasonably well in the internal missing block in which there is surrounding information, but not so well when attempting to extrapolate peripheral structures outside the partial gray segment. In particular, the interpolation method over-flattens estimates near the image boundary, due to the zeroing effect by the four corner points. We note the strong influence of the four corner points to the reconstruction though they occupy

only a small portion of the entire data sites (4 : 346 in this example). In fact, the CDT based method is quite sensitive to the contours of segmentation. As pointed in [28], the distribution of data sites determines the uniqueness of the structure of the CDT, and thus decides the effectiveness of the CDT based approach.

We have also implemented 2D Gaussian filters for interpolation. Figure 10(d) applies a Gaussian filter over FOMFE estimates in the foreground and zero orientations in non-foreground areas. We set the window size $w = 40 \times 40$ and the smoothing parameter $\sigma = 5$. Figure 10(e) applies a Gaussian filter over FOMFE estimates in the entire region. The corresponding window size $w = 40 \times 40$ and $\sigma = 10$. For both Gaussian filters, the FOMFE model coefficients are evaluated based on data inside the available partial fingerprint segments. Comparing the two, Fig. 10(e) presents a better estimation, especially outside the partial fingerprint segment in which the orientation estimates are over-flattened in Fig. 10(d). This is mainly because Fig. 10(d) uses zero orientations as initial estimates in the non-foreground areas. This assignment

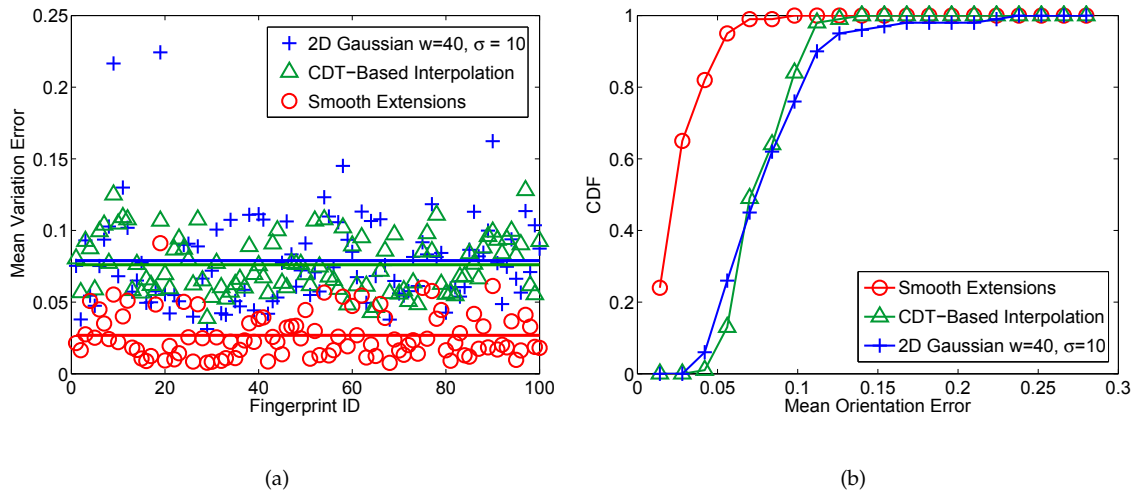


Fig. 11. Comparing orientation estimation accuracy after reconstruction: (a) mean orientation error for every test fingerprint, (b) cumulative distribution function (CDF) with respect to the mean orientation error.

is thus taken into account in the Gaussian smoothing. The results indicate that FOMFE [9] encodes some useful information that is better than null signals for orientation estimation in non-foreground areas. This observation is consistent with (13) in Section 3.2 in which we prove that orientation estimates in the unknown regions are actually affected by both the null space vector and the available data samples (represented by FOMFE) inside the available partial segment(s). Therefore, we will refer the 2D Gaussian filter to the approach demonstrated in Fig. 10(e) and compare the performance with it in all later experiments.

Unfortunately, even the Gaussian filter used in Fig. 10(e) introduces significant deformation to the orientation estimation due to the effect of smoothing. This is evidenced by the shift of singular points with respect to the original detections as shown in the figure. In fact, a larger value of the smoothing parameter helps to obtain a more regularized result for non-foreground areas but also tends to “over-smooth” flows with high curvature in singularity regions. Decreasing the value of the smoothing parameter reduces deformation but may leave the estimates erratic in the unknown region. An example is shown in Fig. 9(b).

Figure 10(f) demonstrates the estimation result from Smooth Extensions. It achieves the best performance among the comparing methods, since the overall ridge flow pattern is reconstructed with remarkably less deformation. Note that the estimated singular points from reconstructed orientation estimates are very close to the original detections, as shown in the figure. Moreover, Smooth Extensions is not restricted to the contour and shape of segmentation as in the CDT-based interpolation. It also eliminates the need of tuning the smoothing parameter to balance the trade-off of regularity-and-deformation as in the Gaussian smoothing. These ad-

vantages make our approach more robust and more accurate for orientation estimation of different partial fingerprints.

It is worth to emphasize that Smooth Extensions is different from normal smoothing techniques. The Smooth Extensions method intends to propagate the existing structural information smoothly and thus “fill” the unknown region progressively with iterative estimates, while the conventional smoothing techniques are usually designed to leave out noise or fine-scaled details in the (existing) data structures. Hence, Smooth Extensions is more suitable for “prediction” in large corrupted areas in which a normal smoothing technique may introduce discrepancies or fail. To quantify the accuracy of orientation estimation, we adopt the following measure [27] to assess the mean orientation estimation error for every fingerprint in our test:

$$\bar{e}_D = \frac{1}{N_D} \sum_{(x,y) \in D} \sin^2(\theta(x,y) - \hat{\phi}(x,y)), \quad (24)$$

where D is the fingerprint area in the original full print image, N_D is the number of samples in D , $\theta(x,y)$ is an orientation angle extracted at a sample point in D , and $\hat{\phi}(x,y)$ is estimated based on the available partial segment using one of the comparing estimation methods demonstrated in Fig. 10. The assessment of (24) is performed for every fingerprint in our test set. Figure 11 reports the experimental results.

Figure 11(a) plots the mean orientation errors from three comparing methods, namely the CDT-based interpolation, the 2D Gaussian filter with $w = 40 \times 40$ and $\sigma = 10$, and Smooth Extensions. It can be observed that, in general, our proposed Smooth Extensions outperforms the other two methods in terms of orientation estimation accuracy by achieving a lower error rate among the three. The average value of mean orientation errors

is 0.0268 by the Smooth Extensions, and 0.0761 and 0.0790 by the CDT interpolation and the Gaussian filter, respectively. Note that the maximum error is *one* when an orientation estimate is orthogonal to the reference.

Figure 11(b) further plots the empirical cumulative distribution function of the mean orientation error from these comparing methods. The interval is 0.014 for the error rate on the x-axis. The figure shows that about 65% of the test prints have a mean orientation error less than 0.028 by using the Smooth Extensions, whereas the percentage drops to nearly 0% for the same error performance by using the CDT interpolation and the Gaussian filter. That is, there is no test object has a mean orientation error less than 0.028.

From the statistical performance shown in Fig. 11, it is difficult to judge if the CDT interpolation outperforms the 2D Gaussian filter. Therefore, we will mainly perform comparison with the 2D Gaussian filter in later experiments for computational benefits. However, the above results do indicate that our proposed method of the Smooth Extensions is more accurate for global ridge orientation estimation based on randomly located image segments of partial fingerprints that may not include the critical singular points.

Although matching ridge orientations alone is by nature not sufficient to verify a fingerprint identity, it can substantially help to narrow down the search range of the potential candidates and thus greatly improve the efficiency of the identification process [7]. This is particularly useful for partial fingerprint identification in which the one-to-one matching is usually much more complex than the conventional minutiae matching. In the following sections, we will examine how the proposed global orientation estimation methods can improve the performance of identifying a partial fingerprint query from fingerprint databases.

5.2 Quality of Partial Fingerprints

For one-to-one fingerprint matching, the image size and resolution are important because they decide the maximum amount of local information detectable in the site. In such cases, matching error raises as the number of available ridge details, e.g. typically minutiae points, decreases [2], [3]. Therefore, from a matcher's perspective, partial fingerprints are regarded as those whose foreground size is less than $0.5'' \times 0.7''$ or in which the number of minutiae points is less than 12 following the forensic requirement of minimum minutiae matching [1], [3], [31].

These matching criteria define the upper bound for quality assessment of partial fingerprints. However, it is not clear how "small" a partial fingerprint segment could be for it to be inherently identifiable. In fact, local ridge features, such as the location of minutiae points, are highly variable - which composes basis of the widely claimed uniqueness of fingerprints. Therefore, it is difficult to define the lower bound for quality assessment

based on requirements of matchers.

We propose to define the lower bound from a new perspective of the retrieval capability. For screening purposes, it is sufficient to compare fingerprints at a coarse level, e.g. based on the global ridge topology pattern, in order to retrieve a relatively short list of candidates for matching. Unlike the local features, the benefit of the global features is that they are somehow "predictable" due to the intrinsic features of ridge topology patterns as we have discussed in Section 2.

Although we understand that fine ridge details in the missing part of a latent fingerprint image cannot be recovered precisely, it is possible to reconstruct *topologically* the same fingerprint global pattern as the original full print for conducting an effective search in the database, and accordingly retrieve a (preferably short) list of the most likely candidates for higher level matches. To the best of our knowledge, there is no literature discussing a similar idea for improving the efficiency and accuracy of candidate retrieval for partial fingerprint identification.

Following the approach, an interesting research question naturally arises: how much information is minimally required to infer the global topology pattern so that a candidate list retrieval scheme can be performed effectively for a partial fingerprint query? In the following, we shall investigate this research question through indexing experiments.

We employ the FVC2002 DB1a database [7] in this test. The database contains 800 optical-scanned fingerprints from 100 identities. The image size is 388×374 pixels and the resolution is $500dpi$. We chose 100 test objects each represents an identity to form the gallery database, such that each gallery fingerprint contains the most complete singularity structures among the 8 impressions. All the gallery prints are registered with respect to the upper most core points via image translation and rotation.

We generate test segments from the gallery prints. Specifically, we segment the singularity areas around cores and deltas in the gallery prints. By varying the segmentation size, we are able to control the size of singularity patterns, i.e. knowledge about the critical structures, and evaluate its impact on reconstruction of the global ridge topology patterns.

Figure 12 demonstrates such a group of examples. The orientation estimates resulting from Smooth Extensions are superimposed on the corresponding partial fingerprint segments. The segmentation is performed with a circular window. As more structural information is included, it can be observed that the topology pattern resembles more closely to the original fingerprint, as shown in the rightmost plot in the figure.

In our experiments, we define R as the window radius for maximum segmentation that covers the entire fingerprint image. In this context, we choose $R = 0.5375''$ given the image resolution and size of fingerprints in the FVC2002 DB1a database. We gradually increase the segmentation radius from 0 to R with a step of $0.04R$. With each segmentation size, we generate a query set

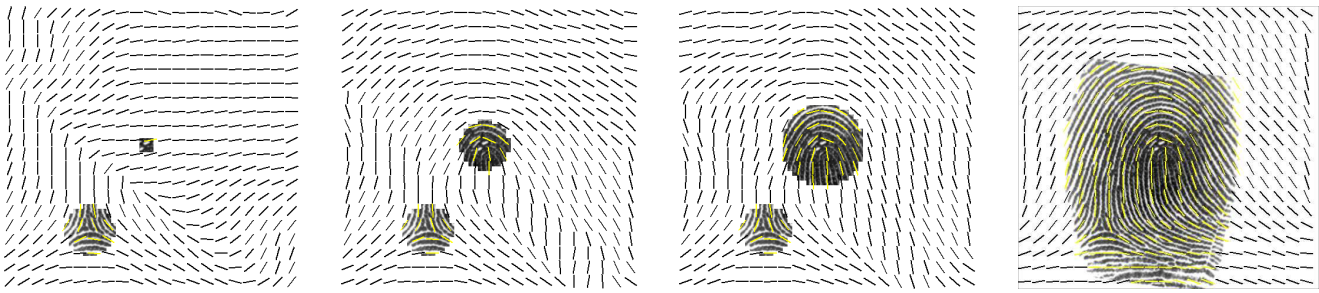


Fig. 12. Impact of core segmentation size on Smooth Extensions.

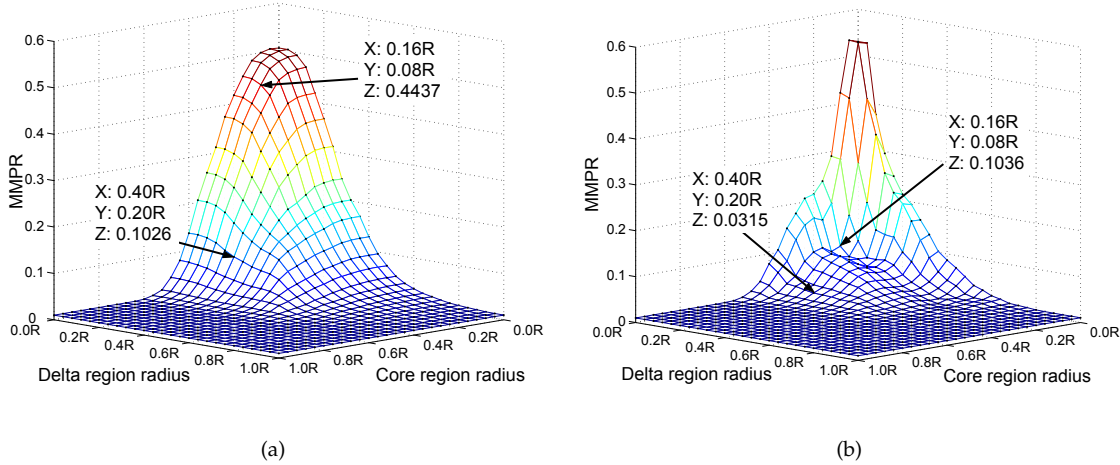


Fig. 13. Partial fingerprint segmentation size on the MMPR retrieval performance: (a) partial representation before reconstruction, (b) global representation after reconstruction.

of 100 partial fingerprints each of different identity. Accordingly, we have $26 \times 26 = 676$ query sets with varying segmentation size in singularity regions. For each query set, we perform a run of search for matching candidates in the gallery database.

We conduct search of matching candidates through fingerprint indexing [9], [10]. The retrieval performance can be measured by two statistical metrics, namely the penetration rate and the error rate (of finding a match). The former is defined as the proportion of database that was probed before a match is found, while the latter measures the retrieval error with respect to the total number of queries in the test [7]. As the probing range increases it is more likely to find the true match. Therefore, we can define the *maximum penetration rate* as that when the retrieval error equals to zero.

To establish the indexing feature space, the Karhunen-Loeve (KL) transform is generally employed to reduce the high dimensionality of the fingerprint indexing feature vector [7]. The feature vector length remained after dimensionality reduction is an important parameter that can affect the indexing performance. The parameter is usually selected at the value that yields the *minimum of the maximum penetration rate* (MMPR) for the test objects in the indexing experiments. The metric indicates

the best retrieval performance for the worst case (of maximum penetration) on average. Ideally, the MMPR performance should be as small as possible for fast retrieval of fingerprint identities.

With the single MMPR metric, we are able to quantify the retrieval performance for each quest set, and find out how “small” (the lower bound of) a partial fingerprint segment could be for it to be inherently identifiable by satisfying certain performance requirement. In this experiment, Smooth Extensions is employed for pattern reconstruction since segmentation is performed around singular points. To evaluate the performance gain, we exploit the model coefficients before and after reconstruction for generating indexing feature vectors. For convenience of expression, we call the former *partial representation* and the latter *global representation*.

As a result, Fig. 13(a) and Fig. 13(b) plot the retrieval performance for all 676 query sets against the gallery database based on the partial representations and the global representations, respectively. In the 3D graphs, the x -axis represents segmentation radius in the core regions, the y -axis represents that in the delta regions, and the z -axis indicates the MMPR performance.

In general, involving more structure information helps to narrow down the search range and hence lower down

the MMPR measure. Comparing the two figures, we see that the MMPR decreases more steeply for the global representation. This indicates that our pattern reconstruction scheme can improve the retrieval performance for partial fingerprint segments with the same amount of structure information. For instance, when the core segmentation radius $X = 0.40R$ ($0.215''$) and the delta segmentation radius $Y = 0.20R$ ($0.107''$) the partial representation yields a 10% MMPR performance while the global representation can reach a much lower rate of 3%. Figure 13(b) shows that, to achieve the same 10% MMPR performance the global representation requires much less structure information for $X = 0.16R$ ($0.086''$) and $Y = 0.08R$ ($0.043''$). With the same segmentation size, however, the partial representation yields a much worse MMPR performance by requiring 44% of the database to be probed, as shown in Fig. 13(a).

In Fig. 13, we also notice that the MMPR measure decreases faster along the x -axis. This also indicates that the core information is more critical than the delta information. The next section will further investigate how well the proposed algorithms can improve the indexing performance for partial fingerprints of which singularities are missing.

5.3 Retrieval Performance after Reconstruction

In this section, we evaluate the retrieval performance of the proposed reconstruction schemes for identifying difficult partial fingerprints of which one or more singularities are missing. Our experiments are conducted on the NIST SDB14 database [29]. We use the last 2700 F prints to compose the gallery database in which all gallery prints are registered to the image center before indexing.

For queries, we first randomly select one hundred S prints such that there are at least one core and one delta exhibit in the corresponding gallery prints. As in the previous experiment, we segment singularity regions in the S prints and use only the structure information in the partial segments for tests. We define the maximum segmentation radius R as $0.700''$, given the image size (480×512 pixels) and resolution ($500dpi$). We then vary the core region radius from $0.16R$ ($0.112''$) to $0.60R$ ($0.421''$), and the delta radius from $0.16R$ ($0.112''$) to $0.80R$ ($0.561''$). As a result, we obtain 12 query sets by segmentation around cores, namely the *Core Groups*, and 17 query sets by segmentation around deltas, namely the *Delta Groups*. In total, there are 29 query sets each containing 100 partial fingerprint segments for identification.

The partial fingerprint queries must also be registered to the image center before indexing. For Core Groups, it is not difficult to apply normal singular point detection algorithms to find the core points as they already exist in the partial fingerprint segments. For Delta Groups, however, we have to “predict” the missing core points after reconstruction. The estimated global orientation

field is then registered to the image image center with respect to the predicted core points. The blank areas after translation are supplemented by Smooth Extensions.

We implemented three comparative orientation reconstruction methods, namely the 2D Gaussian filter (with $w = 40 \times 40$ and $\sigma = 10$), the cosine peripheral model, and the fluid peripheral model. We tested their corresponding global representations after reconstruction for indexing experiments. We have also tested the partial representations from the FOMFE model before reconstruction. Figure 14 plots the individual test results from all four comparing methods for the Core Groups and Delta Groups, respectively.

When the segmentation size is small, the three reconstruction methods in general perform better than the original partial representations by being able to obtain lower penetration rates. As the segmentation size increases, the MMPR curves tend to converge to the same performance level. This observation agrees with our analysis in Section 3.1, which indicates that the partial representations can approximately describe the overall topology structures when the partial segment is large enough to include core region with radius exceeding $0.60R$ ($0.421''$), as shown in Fig. 14(a).

For Delta Groups, since critical core points are missing and registration must rely on estimated core points after reconstruction, the performance is generally worse and less stable than that of a Core Group with the same segment size. However, the convergence trend also exhibits in Fig. 14(b) and it is clear that our proposed ridge topology reconstruction is able to improve retrieval performance significantly for partial fingerprint identification.

In both figures, the fluid peripheral and the cosine peripheral models in general outperform the 2D Gaussian filter approach. This is particular significant for the Delta Groups shown in Fig. 14(b). The phenomena indicates that incorporating the a priori knowledge of ridge smoothness and peripheral arches can substantially improve the performance of global orientation estimation. Note that the Gaussian filter introduces discrepancies when the effective area increases due to the over-smoothing effect by the filter parameters.

Comparing the two incorporation methods, the fluid peripheral model performs better by being able to yield a lower penetration rate over the database. This is particularly obvious for the Core Groups. For instance, the fluid peripheral yields about 21% MMPR for the Core Group with a $0.24R$ ($0.168''$) segmentation radius, as shown in Fig. 14(a). The performance gain is about 10% over the cosine peripheral method, about 13% over the 2D Gaussian filter, and almost 40% over partial representations before reconstruction. For the Delta Groups, the two incorporation methods have close performance while the fluid peripheral slightly performs better.

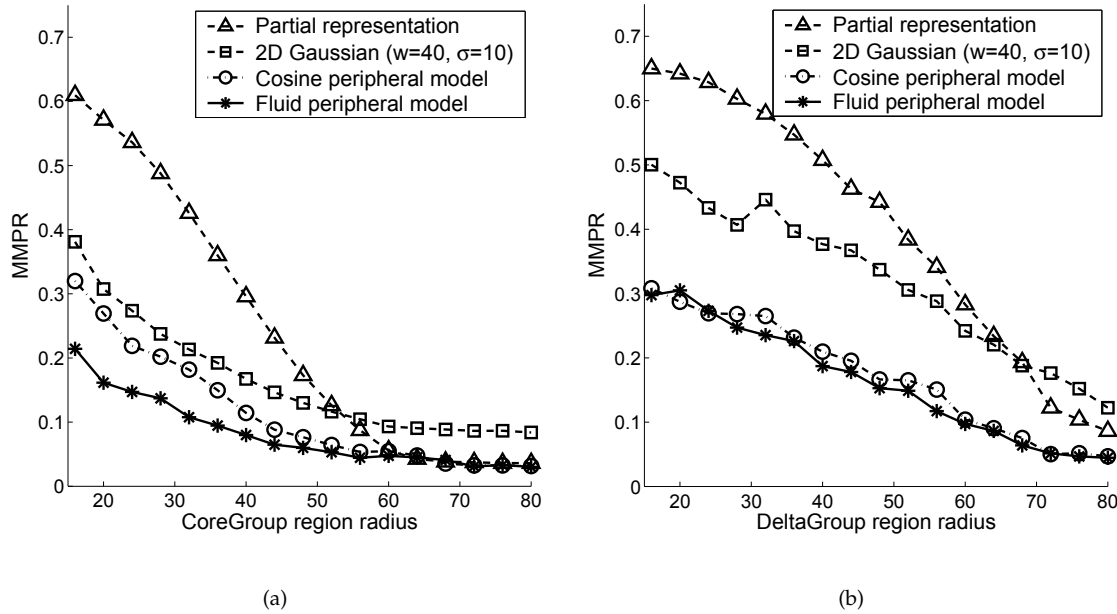


Fig. 14. MMPR with varying segmentation size around singularities: (a) Core Groups; (b) Delta Groups.

6 CONCLUSION

Partial fingerprint identification has been a critical challenge to date. Existing partial fingerprint algorithms mainly focus on one-to-one verification by assuming that candidate lists for matching have already been established. However, effective candidate list reduction is an important and difficult task for partial fingerprint identification. This has led us to study the global ridge orientation reconstruction problem for partial fingerprint identification.

Our approach is to describe the reconstruction problem as an inverse model. As a result, we are able to define the general solution space for all possible solutions that can maintain data fidelity in the existing segments. The solution space is further damped by incorporating the a priori knowledge of global ridge topologies, namely ridge smoothness and peripheral arches. To that end, we have developed two algorithms for estimating the unknown orientation structures. The algorithms can be used individually depending on the available information. Our results from statistical experiments have shown that the proposed approach can effectively reduce the size of candidate lists for matching, and thus can significantly improve the retrieval efficiency for partial fingerprint identification.

ACKNOWLEDGMENTS

The authors would like to thank Dr. Geppy Parziale from Cogent Systems, Inc. for helpful discussions during the 5th Biometrics Summer School held in Alghero, Italy. We are also grateful to anonymous reviewers for their many valuable suggestions. The work in this paper was supported by the Australian Research Council (ARC) Link-

age Project LP0455324. The research of Jiankun Hu is supported in part by ARC Discovery Project DP0985838 and Linkage Project LP100100404.

REFERENCES

- [1] T. Jea and V. Govindaraju, "A minutiae-based partial fingerprint recognition system," *Pattern Recognition*, vol. 38, no. 10, pp. 1672–1684, Oct 2005.
- [2] G. Fang, S. Srihari, H. Srinivasan, and P. Phatak, "Use of ridge points in partial fingerprint matching," in *Biometric Technology for Human Identification IV: Proc. SPIE*, Orlando, FL, Apr. 2007.
- [3] Y. Chen and A. K. Jain, "Dots and incipients: extended features for partial fingerprint matching," in *Biometric Consortium Conference*, Baltimore, MD, Sep 2007.
- [4] "Concept of operations (conops) for evaluation of latent fingerprint technologies (elft)," National Institute of Standards and Technology (NIST), Tech. Rep., Jun. 2007.
- [5] J. Feng and A. K. Jain, "Filtering large fingerprint database for latent matching," in *Proc. Int. Conf. on Pattern Recognition (ICPR'08)*, Dec. 2008, pp. 1–4.
- [6] C. Watson, M. Garris, E. Tabassi, C. Wilson, R. McCabe, and S. Janet, "User's guide to NIST fingerprint image software 2 (NFIS 2)," National Institute of Science and Technology (NIST), Software manual 2, 2001.
- [7] D. Maltoni, D. Maio, A. K. Jain, and S. Prabhakar, *Handbook of Fingerprint Recognition*. New York: Springer-Verlag, 2003.
- [8] M. F. Card, "NIST special database 14." [Online]. Available: <http://citeseer.ist.psu.edu/247429.html>
- [9] Y. Wang, J. Hu, and D. Phillips, "A fingerprint orientation model based on 2D Fourier expansion (FOMFE) and its application to singular-point detection and fingerprint indexing," *IEEE Trans. Pattern Anal. Machine Intell.*, vol. 29, no. 4, pp. 573–585, Apr. 2007.

[10] A. Lumini, D. Maio, and D. Maltoni, "Continuous versus exclusive classification for fingerprint retrieval," *Pattern Recognition Letter*, vol. 18, no. 10, pp. 1027–1034, 1997.

[11] J. Boer, A. Bazen, and S. Gerez, "Indexing fingerprint database based on multiple features," in *Proc. Workshop on Circuits, Systems and Signal Processing*. Springer Verlag, Nov 2001, pp. 58–66.

[12] R. Cappelli, D. Maio, and D. Maltoni, "Multispace KL for pattern representation and classification," *IEEE Trans. Pattern Anal. Machine Intell.*, vol. 23, no. 9, pp. 977–996, Sep 2001.

[13] J. Li and Y. Yau, "Prediction of fingerprint orientation," in *Proc. Int. Conf. on Pattern Recognition (ICPR'04)*, vol. 4, Aug. 2004, pp. 436 – 439.

[14] B. Sherlock, D. Monro, and K. Millard, "Fingerprint enhancement by directional Fourier filtering," in *IEE Proc. Vision, Image and Signal Processing*, vol. 141, no. 2, Apr. 1994, pp. 87–94.

[15] P. Vizcaya and L. Gerhardt, "A nonlinear orientation model for global description of fingerprints," *Pattern Recognition*, vol. 29, no. 7, pp. 1221–1231, 1996.

[16] S. Dass, "Markov random field models for directional field and singularity extraction in fingerprint images," *IEEE Trans. Image Processing*, vol. 13, no. 10, pp. 1358–1367, 2004.

[17] J. Zhou and J. Gu, "A model-based method for the computation of fingerprints orientation field," *IEEE Trans. Image Processing*, vol. 13, no. 6, pp. 821–835, 2004.

[18] A. Rao and R. Jain, "Computerized flow field analysis: oriented texture fields," *IEEE Trans. Pattern Anal. Machine Intell.*, vol. 14, no. 7, pp. 693–709, Jul. 1992.

[19] R. Ford and R. Strickland, "Nonlinear phase portrait models for oriented textures," in *Proceedings of Computer Vision and Pattern Recognition*. IEEE computer society, Jun. 1993, pp. 644 – 645.

[20] W. Yau, J. Li, and H. Wang, "Nonlinear phase portrait modeling of fingerprint orientation," in *IEE Proc. Control, Automation, Robotics and Vision Conference*, vol. 2, Dec. 2004, pp. 1262–1267.

[21] R. Gonzalez and R. Woods, *Digital Image Processing*. Prentice Hall, 2001.

[22] W. Press, S. Teukolsky, W. Vetterling, and B. Flannery, *Numerical Recipes in C: the Art of Scientific Computing*. New York: Cambridge University Press, 1992.

[23] W. Menke, *Geophysical Data Analysis: Discrete Inverse Theory*. New York: Academic Press, Inc., 1984.

[24] M. Deal and G. Nolet, "Nullspace shuttles," *Geophysical Journal International*, vol. 124, no. 2, pp. 372–380, 1996.

[25] R. Cappelli, A. Lumini, D. Maio, and D. Maltoni, "Fingerprint image reconstruction from standard templates," *IEEE Trans. Pattern Anal. Machine Intell.*, vol. 29, no. 9, pp. 1489–1503, Sep. 2007.

[26] L. M. Milne-Thomson, *Theoretical Hydrodynamics*. New York: Dover Publications, 1996.

[27] P. Perona, "Orientation diffusions," *IEEE Trans. Image Processing*, vol. 7, no. 3, pp. 457–467, Mar. 1998.

[28] Q. Zhang and H. Yan, "Fingerprint orientation field interpolation based on the constraint delaunay triangulation," *International Journal of Information and Systems Sciences*, vol. 3, no. 3, pp. 438–452, 2007.

[29] NIST special databases and software. [Online]. Available: <http://www.itl.nist.gov/iad/894.03/databases/defs/dbases.html#finglist>

[30] G. Nielson, H. Hagen, and H. Muller, *Scientific Visualization: Overviews, Methodologies, and Techniques*. IEEE Computer Scientific Press, 1997.

[31] V. Govindaraju, "Advances in fingerprint recognition at CUBS," in *Proc. Int. Workshop on Document Analysis*, Koldata, 2005, pp. 149–174.



Yi Wang received the BE degree in 2002 from the School of Electronic and Information Engineering at South China University of Technology, Guangzhou, China, the ME degree in telecommunications in 2003 from the University of Melbourne, and the PhD degree in computer science in 2009 from RMIT University, Melbourne, Australia. From 2003 to 2004, she was a research assistant with the Department of Electrical and Electronic Engineering at the University of Melbourne, and with the Department of Electronic Engineering at City University of Hong Kong. She is now a postdoctoral research associate with the School of Mathematics and Statistics at the University of New South Wales, Sydney, Australia. Her research interests include biometrics and statistical pattern recognition. She is a member of the IEEE.



Jiankun Hu is an associate professor at the School of Computer Science and Information Technology, RMIT University, Australia. His major research interest is in computer networking and computer security, especially biometric security. He has been awarded four Australia Research Council grants. He served as Security Symposium Co-Chair for IEEE GLOBECOM 08 and IEEE ICC09. He was Program Co-Chair of the 2008 International Symposium on Computer Science and Its Applications. He has been on editorial board for following journals: *Journal of Network and Computer Applications*, Elsevier; *Journal of Security and Communication Networks*, Wiley; and *Journal of Wireless Communication and Mobile Computing*, Wiley. He is the lead Guest Editor of a 2009 special issue on biometric security for mobile computing, *Journal of Security and Communication Networks*, Wiley. He received a Bachelors degree in industrial automation in 1983 from Hunan University, P.R. China, a Ph.D. degree in engineering in 1993 from the Harbin Institute of Technology, P.R. China, and a Masters degree for research in computer science and software engineering from Monash University, Australia, in 2000. In 1995 he completed his postdoctoral fellow work in the Department of Electrical and Electronic Engineering, Harbin Shipbuilding College, P.R. China. He was a research fellow of the Alexander von Humboldt Foundation in the Department of Electrical and Electronic Engineering, Ruhr University, Germany, during 1995–1997. He worked as a research fellow in the Department of Electrical and Electronic Engineering, Delft University of Technology, the Netherlands, in 1997. Before he moved to RMIT University Australia, he was a research fellow in the Department of Electrical and Electronic Engineering, University of Melbourne, Australia. More details could be found from his homepage at <http://goanna.cs.rmit.edu.au/jiankun/>.